ERDC/CHL CHETN-IV-130
August 2022

US Army Corps of Engineers®

Method to Evaluate Vessel Wake Forces on Wetland Scarps

by Richard Styles, Rachel L. Bain, and Anthony M. Priestas

PURPOSE: This Coastal and Hydraulics engineering technical note (CHETN) presents a methodology to compute normal forces on wetland perimeters with vertically scarped edges. The approach uses an empirical algorithm that predicts the normal force given the offshore vessel wake height, period, and water depth at a given point. Wave impact forces are measured using load cells, which have not been applied previously to marsh settings. Load cell and vessel wake measurements from two field sites are combined to generate an empirical transfer function relating forces to incoming vessel wake characteristics.

INTRODUCTION: It is well known that coastal wetlands serve important environmental functions such as nutrient and chemical exchange between terrestrial and marine environments, as well as habitat for a wide variety of aquatic organisms. Wetlands are also recognized as natural buffer zones to help protect coastal communities from storm impacts and flooding (Gedan et al. 2011; Wamsley et al. 2010). Considering their ecological benefit and likely role in flood and storm protection, wetland restoration projects in heavily impacted areas have been a major focus around the globe (Kumar 2012).

Wetland restoration projects in high-energy environments such as tidal channels and exposed shorelines (e.g., wind waves) are susceptible to accelerated erosion of the recently placed material. Long-term edge erosion through wind-generated wave attack is well documented and remains an important consideration when designing and executing wetland restoration projects (Marani et al. 2011; Bloemendaal et al. 2021; McLoughlin et al. 2015). As such, developing mitigation strategies to reduce the erosional impacts helps to ensure that wetland restoration projects meet long-term sustainability projections. Vessel-generated waves, especially the surge that can produce wave heights of 0.5 to 1.0 m*, have been implicated as a contributing cause of erosion along exposed shorelines (Houser 2011; 2010; Maynord 2007). In interior regions, where wetlands are sheltered from waves originating in the navigation channel, the major source of wave energy is hypothesized to come from recreational vessels.

Even though recreational craft typically do not generate waves as large as commercial vessels, they are able to directly impact vulnerable regions of the wetland interior that would otherwise receive no waves from vessels operating in navigation channels. Restoration projects that place sediment within the wetland interior, where tide and wave energy is weak, may still need to consider the effects of recreational craft, especially in highly populated areas that receive a large volume of boat traffic. Considering that recreational vessel use is on the rise globally (Burgin and Hardiman 2011), coastal plain saltmarshes can expect to see an increase in the number of small

* For a full list of the spelled-out forms of the units of measure used in this document, please refer to *US Government Publishing Office Style Manual*, 31st ed. (Washington, DC: US Government Publishing Office 2016), 248-52, https://www.govinfo.gov/content/pkg/GPO-STYLEMANUAL-2016/pdf/GPO-STYLEMANUAL-2016.pdf.

craft and greater potential for accelerated erosion along exposed marsh perimeters. Better constraining the forces responsible for erosion and how they vary as a function of vessel operations is a key area of research needed to better plan and execute wetland restoration projects.

BACKGROUND: The wake envelope generated by an individual vessel varies widely as a function of vessel type and operating conditions (e.g., speed, draft, hull design, length, and beam). Widely used phase-averaged wave models, which assume a statistically steady wave train, are consequently insufficient to represent the erosive potential of vessel wakes. Simplified vessel wake models have been developed in the past to investigate the relative contribution of vessel wake to other sources of energy such as river flow, wind waves or tides (Sorensen 1997; Maynord et al. 2008; Styles and Hartman 2018). In this scenario, the cumulative energy from vessel wakes over a given timeframe can be compared to the equivalent energy of another forcing (e.g., the tidal flow). If the wave energy flux is dwarfed by the tidal energy, then it is assumed that the vessel wake does not substantially contribute to shoreline erosion. This simple approach only requires energy calculations from these different sources, which can be accomplished using flow and wave sensors. However, energy weighting does not provide estimates of shoreline erosion. Rather, this method only predicts the energy flux, which is used as a surrogate for erosion potential. Energy weighting is often used in areas with limited data collection to help eliminate or further refine possible engineering alternatives in preparation for a more focused study. Furthermore, quantifying energy fluxes from various sources does not consider the spatial distribution of where those energies are dissipated and how that relates to erosion potential.

A higher-order approach is to combine long-term measurements of shoreline retreat and simultaneous estimates of wave power to create a regression model (Leonardi et al. 2016; Priestas et al. 2015; Schwimmer 2001). Wave energy dissipated during breaking is assumed to be directly correlated to shoreline erosion. While the regression model provides an estimate of shoreline loss, it also exhibits a large degree of uncertainty because various factors contributing to erosion are not quantified. These include geotechnical properties of the soil, soil retention and strength properties of vegetation, biological disturbances, and the effect of water level on wave and current impacts (Mcloughlin et al. 2015). Furthermore, the shear stresses responsible for sediment mobilization and the impact forces that lead to mass failure are not computed directly but rather are represented implicitly in the regression coefficients. Higher-order numerical modeling can provide direct estimates of erosion; however, data to validate and improve sediment transport and erosional algorithms, especially in a multiphase flow simulation where slumping and undercutting are the primary modes of long-term edge erosion, is lacking. Even if the wave and geotechnical properties are known, the measured erosion rate sometimes fails to produce a direct correlation to the wave power (Bloemendaal et al. 2021). This is further compounded due to the transient vessel wake packet, which likely cannot be treated using the same linear statistical methodologies routinely applied to wind waves.

In tide-dominated coastal plain wetlands, wave forces on exposed shorelines vary as a function of tidal stage. Around low tide, waves are more likely to break due to shoaling on the mud flat that terminates at the base of the scarp. At mid-tide, the vertical scarped face causes a combination of wave breaking and reflection; consequently, erosion models based on the total energy dissipation argument may be less valid because some of the incoming energy is redirected offshore. At high tide, the marsh platform is subjected to overtopping waves, where the waves pass over the scarp to penetrate the marsh interior, which means less energy is dissipated on the scarp. Numerical

modeling on terraced scarps showed maximum forces when the water level was just below the elevation of the mash platform (Tonelli et al. 2010). However, field data were not available to confirm their result.

Because of their ecological benefits and potential costs savings, natural and nature based features (NNBFs) are gaining more acceptance as shore protection measures in coastal wetlands (Bridges et al. 2015). Given that NNBF structures vary widely in construction materials and function, there is very little design criteria for establishing performance testing that satisfies structural integrity requirements as well as lifecycle performance metrics. Load cells are routinely applied to measure direct wave impacts including surge and breaking forces in designing and testing hydraulic structures and could likewise quantify loadings on NNBF designs. Understanding the direct impact of waves on marine organisms (clam beds, oyster reefs) can also provide insight into ecosystem habitat resilience as well as structural functionality of these natural sediment stabilizers.

Improving numerical model predictions, constraining the physics of marsh edge erosion in areas with heavy vessel traffic, and evaluating hydraulic loadings on NNBF wave damping technologies require datasets of the key physical processes including wave characteristics and the resulting impact forces. The transient wave packet, which is modulated by the wave energy flux envelope, introduces added complexity because of the large change in wave characteristics between the source and the point of impact, not to mention the variability in impact forces associated with tidal stage and vessel operations (speed, draft, beam, length). The purpose of this CHETN is to present a force transfer function that can be used to predict wave loadings from vessels given the offshore wave characteristics. Field data collection of vessel wake and simultaneous vertical force loadings at the shoreline are presented followed by the empirical model development. The model is validated using datasets from two marsh field settings with scarped edges.

LOAD CELLS: The load cells used in the study are submersible s-type strain gauges (model HRS-1K) with a full capacity of 1000 lb (4448 N) in compression and tension. The full-scale output of the load cells is 2 mV/V of excitation and provide a highly linear response. Non-linearity in the output is reported by the manufacturer as 0.1% of full scale and thus capable of resolving 0.5 lb (2.2 N) forces. Each load cell is wired to a signal amplifier (Futek IAA100) set to 10 mV/V of output. The output voltage is captured using a custom-built data acquisition system sampling at 3200 Hz. A custom array system was also developed to deploy the load cells in the field; a schematic drawing of a three-panel, nine-load cell array is shown in Figure 1. The modular design of the array allows the panels to accommodate various scarp heights. A single panel consists of a vertical array of three load cells. The load cells are firmly secured to the rear mounting plate on one side while the other end is freestanding within a hole of slightly larger diameter. Affixed to the front of each load cell is a 7.5 cm diameter loading plate to absorb the wave forces. This plate diameter was considered large enough to adequately register relatively small compressive forces from vessel wakes yet small enough not to introduce off-axis loading. When assembled, the loading plates are flush with the front panels. The arrays were firmly secured to the face of the scarp using two 0.7 m screw earth anchors per array, as any play between the array and scarp would underestimate wave forces.

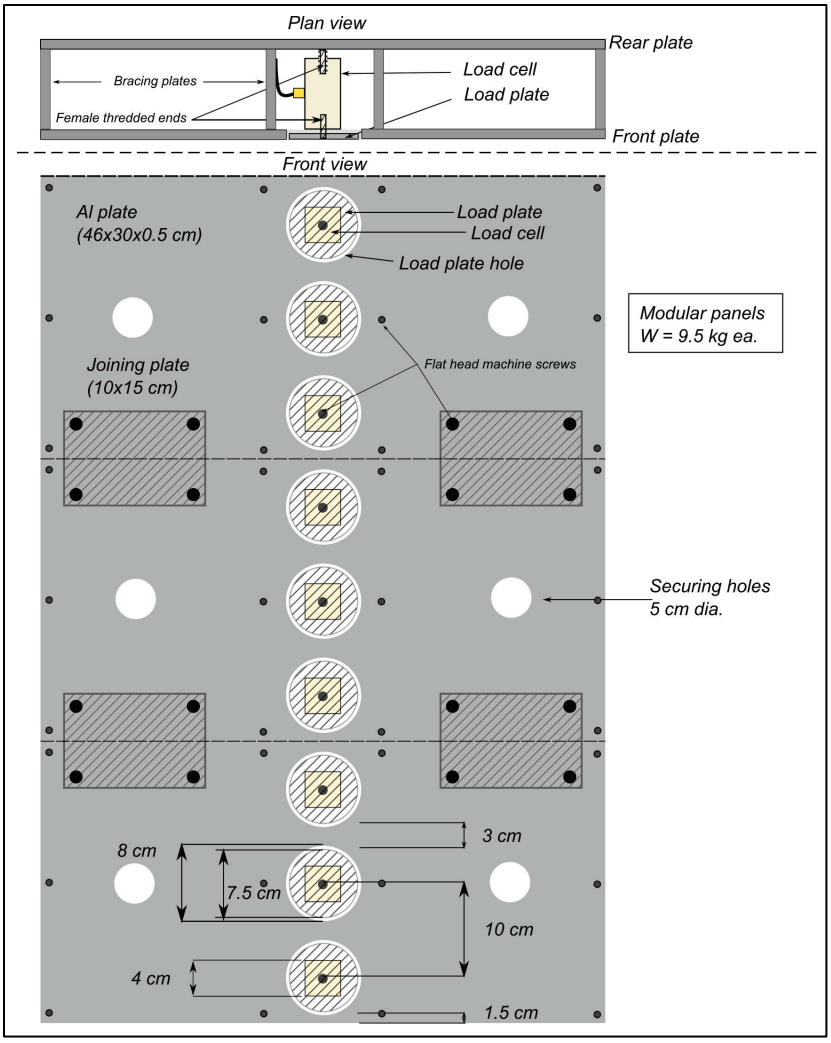

Figure 1. Schematic diagram of modular load cell array shown in plan view (top image) and front view (bottom image).

FIELD TEST SITES: Two field experiments were conducted, one near Cocodrie, Louisiana, and one near St. Augustine, Florida. The Cocodrie study (04–05 August 2020) was conducted along a scarped shoreline from an eroded remnant of a dredge mound near Mile 11 of the southern entrance of the Houma Navigation Canal (Figure 2). A necessary condition for the wave impact measurements includes a scarped shoreline with a minimum relief of 35 to 40 cm (the height of one load cell panel) (Figure 1). A survey of adjacent marshes in the area revealed marsh shorelines with excessively low scarp reliefs and low platform elevations. However, the elevation of the dredge mound is superelevated relative to surrounding marshes, and the soil consists of well-compacted silt and clay that contrasts with the typical marsh shorelines in the area. Consequently, this shoreline's higher elevation, soil character, and accessibility made it well suited for wave impact tests. The scarp height was 1 m, and the slope of the mudflat was approximately 0.1. Tides are semidiurnal with a tidal range of approximately 0.3 m. Two load cell panels (collecting data at 3200 Hz) and a Paros pressure sensor (16 Hz) were used at this site (Figure 2a-d). The panel faces of the load cell arrays were oriented at slight angles to the main channel (10°), and 10°–14° off vertical (Figure 2d) caused by the uneven geometry of the shoreline. A Nortek Signature 1000 acoustic Doppler current profiler (ADCP) was also deployed in the navigation channel, though

those data are not considered for this effort. The Florida study (16–28 September 2020) was conducted along the Intracoastal Waterway (IWW) within the Mantanzas River estuary near Marineland, FL, Flagler County, which cuts through backbarrier and fringing marshlands of the Guana Tolomata Matanzas Research Reserve (Figure 2e). The tidal regime is semidiurnal with mean neap and spring tide ranges of approximately 1.0–1.8 m near the Matanzas Inlet (Gallivan and Davis 1981), though they appear to be somewhat modulated near the study site based on recent water level measurements. The measured near-surface current velocities were nearly symmetrical with speeds of 0.4–0.5 m/s, north and south. Channel margins of the IWW consist of saltmarsh, dredge spoil islands, uplands, and intertidal mud flats and shoals. Elevated shoreline margins will often have a scarped morphology, which are indicative as an erosive feature. At the study site, the marsh scarp height was approximately 40 cm, and the adjacent slope was approximately 0.13. Three load cell arrays (A1, A2, A3) were mounted vertically into the face of the scarped shoreline, spaced approximately 1 m on center (Figure 2g) with panel faces perpendicular to the channel. Two other pressure sensors and two Nortek Signature 1000 ADCPs were also deployed, but those data are likewise not considered in this effort.

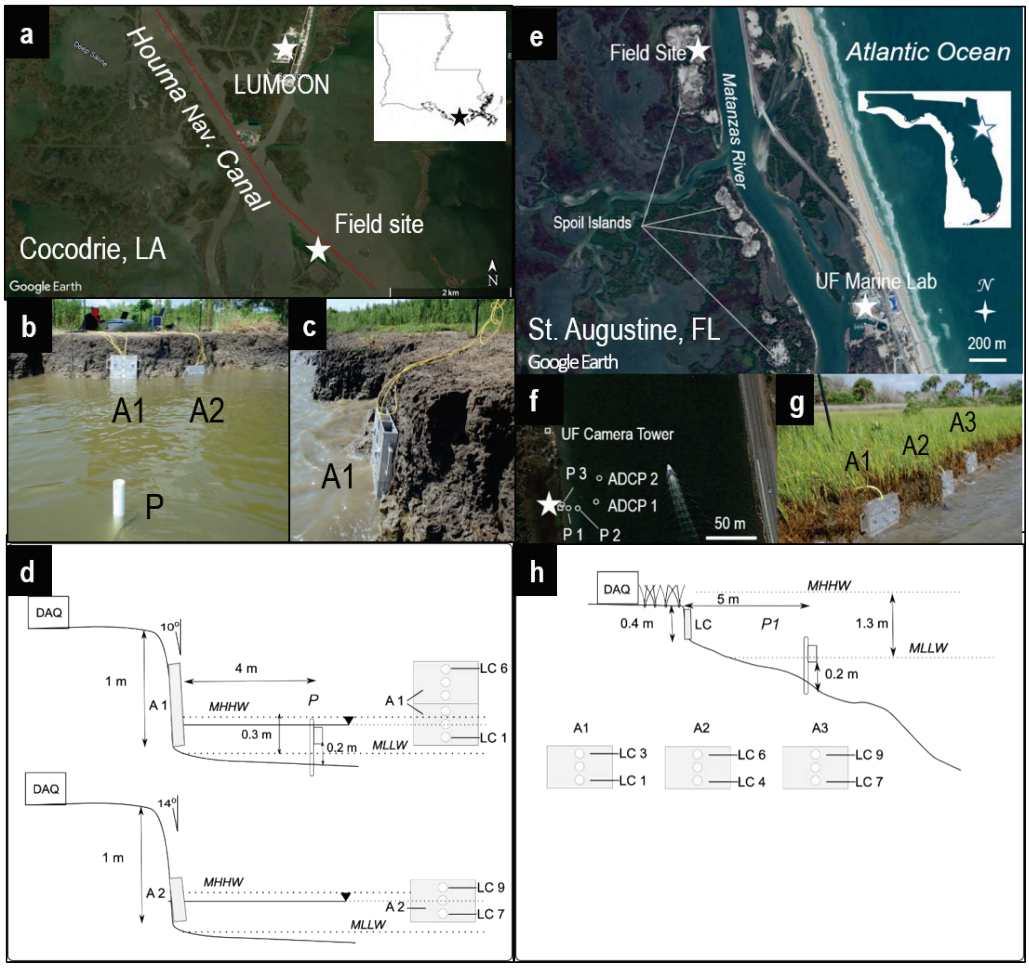

Figure 2. Location maps of the field sites at Cocodrie, LA (a-d) and the Matanzas River, FL (e-h). Instruments consist of Paros Digiquartz pressure sensors (P) and load cell arrays (A1–A3). Wave analysis for the Florida site is restricted to data derived from the pressure sensor closest to the shoreline (P1, shown in f and h).

WAVE ENERGY AND IMPACT FORCE THEORY: Wave conditions during each wake event were calculated as follows. The wave height H_i [m] for the i^{th} half-oscillation (i.e., crest or trough) (Figure 3a) was defined as twice the vertical distance between the extreme elevation and mean water level h during the wake, with the oscillations determined using a zero-crossing algorithm. For a wake event beginning at timestamp t_{start} and ending at timestamp t_{end}, the peak wave period T_p [s] was assigned based on the frequency of the maximum-amplitude wavelet coefficient recorded between t_{start} and t_{end} (Figure 3b). Using these values, the instantaneous energy flux corresponding to the i^{th} half-oscillation was calculated as

$$(\text{energy flux})_i = \frac{\pi}{8T_p k}\rho g H_i^2 \left(1 + \frac{2kh}{\sinh(2kh)}\right) \left[\frac{\text{J}}{\text{m} \cdot \text{s}}\right] \tag{1}$$

where h [m] is the mean depth of water column during the wake event and k [m^{-1}] is the wavenumber determined from T_p and h. Multiplying Equation 1 by $T_p \rho^{-1} g^{-1} h^{-3}$ gives

$$(\text{nondimensional energy flux})_i = \frac{\pi}{8kh}\left(\frac{H_i}{h}\right)^2 \left(1 + \frac{2kh}{\sinh(2kh)}\right) [-]\,. \tag{2}$$

The total energy of a wake event containing N half-oscillations was then calculated as

$$\text{total energy} = \tfrac{1}{2} T_p \sum_{i=1}^{N} (\text{energy flux})_i \tag{3a}$$

$$= \frac{\pi \rho g}{16k}\left(1 + \frac{2kh}{\sinh(2kh)}\right) \sum_{i=1}^{N} H_i^2 \left[\frac{\text{J}}{\text{m}}\right]. \tag{3b}$$

The factor of ½ in Equation 3a accounts for the double-counting of each full-phase oscillation due to the measurement of H_i at both the crest and the trough. Dividing Equation 3b by $\rho g h^3$ gives

$$\text{nondimensional total energy} = \frac{\pi}{16kh}\left(1 + \frac{2kh}{\sinh(2kh)}\right) \sum_{i=1}^{N} \left(\frac{H_i}{h}\right)^2 [-]\,. \tag{4}$$

Load Cell Analysis. Analysis of the load cells is performed using a time series of forces $F(t)$ [N]. The peak load was calculated based on measurements from each individual load cell:

$$F_{max} = \frac{1}{M} \sum_{i=1}^{M} (F_{max})_i \ \text{[N]} \tag{5}$$

where $(F_{max})_i$ is the peak force recorded by the i^{th} load cell during a given wake event (see example in Figure 3b. The number of load cells, M, ranged between 3 and 9 depending on date and location.

The measured peak force was then converted to an impact pressure and nondimensionalized by hydrostatic pressure:

$$\text{nondimensional } P_{max} = \frac{F_{max}}{A_{plate}\rho g h} \; [-] \tag{6}$$

where A_{plate}=0.0046 m^2 is the area of one face plate. To calculate the total compressive impulse of the wake event, all tension forces were set to zero:

$$F_{\text{compress}}(t) = \begin{cases} 0, F(t) < 0 \\ F(t), F(t) \geq 0 \end{cases} \tag{7}$$

The total compressive impulse was then defined as

$$\text{impulse} = \int_{t_{start}}^{t_{end}} F_{\text{compress}}(t)\, dt \;\; [\text{N} \cdot \text{s}] \tag{8}$$

which corresponds to the blue-shaded area in Figure 3b. As a nondimensional value, this becomes

$$\text{nondimensional impulse} = \frac{\text{impulse}}{A_{plate}\rho g h T_p} \; [-]\,. \tag{9}$$

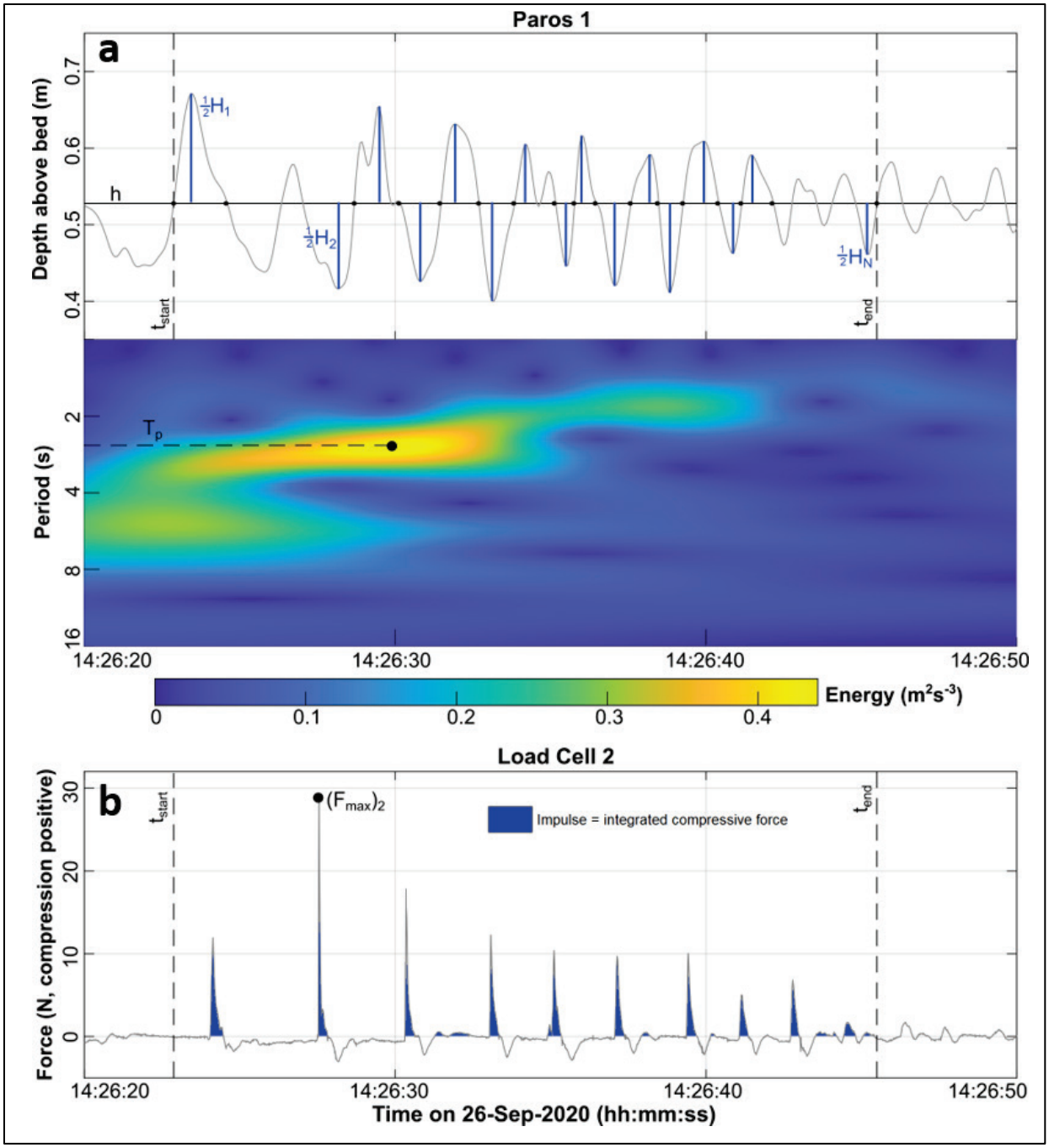

Figure 3. Illustration of variables used to define the wave height-force relationship. The upper frame shows the record of water surface elevation from Paros 1, with its wavelet transform below. The lower frame displays the corresponding time series from Load Cell 2. The height H for each of N half-oscillations is defined as twice the distance between the extreme elevation and mean water level h. The start and end times of the event (tstart and tend) were defined using a zero-crossing algorithm, which required a minimum amplitude of 5 cm and a minimum time of 0.5 s between zero crossings. The peak period *Tp* corresponds to the maximum-amplitude wavelet coefficient during the wake event. The maximum force from the *Mth* load cell, (*Fmax*)*M*, is the maximum compressive force occurring between *tstart* and tend. The impulse is then calculated as the time integral of all compressive forces between *tstart* and tend, which corresponds to the blue shaded area of the lower plot.

Wave Force Theory. Oumeraci et al. (2001) and Cuomo et al. (2010) proposed the following equation to compute the maximum shock pressure, P_{max}, as a function of the wave height:

$$P_{max} \cdot \Delta x = \beta \rho g h^2 \left(\frac{H_{sig}}{h}\right)^{\zeta} \tag{10}$$

where H_{sig} is the significant wave height at the toe of the scarp, Δx=1 is the unit width of the scarp (which is necessary to maintain dimensional homogeneity), and β and ζ are fitted parameters. Cuomo et al. (2010) report values of β=15 and ζ=3.134. The maximum shock pressure during the wake event is calculated as

$$P_{max} = \frac{F_{max}}{A_{plate}} \tag{11}$$

where F_{max} is the peak load recorded by the load cell array during the wake event, and A_{plate}=0.0046 m^2 is the area of the circular face plate. To evaluate Equation 10 using data from Cocodrie and St. Augustine, H_{sig} was assumed to equal the maximum-magnitude value of H_i during each wake event at the Paros instrument nearest the scarp (i.e., Paros 1 at St. Augustine; only one Paros was deployed at Cocodrie). The water depth h was taken as the mean water depth during the wake event at the same Paros instrument. This introduces some uncertainty into the calculations because the Paros instrument was 5 m offshore of the marsh scarp whereas the Equation 10 assumes values of H_{sig} and h at the scarp face. After rearranging Equation 10 and taking the log transform,

$$\log_{10}\left(\frac{P_{max} \cdot \Delta x}{\rho g h^2}\right) = \log_{10}\beta + \zeta \log_{10}\left(\frac{H_{sig}}{h}\right), \tag{12}$$

best-fit values of β between 0.46 and 2.80 and best-fit values of ζ between 0.87 and 1.52 were determined using linear least squares (Figure 5).

FIELD RESULTS AND TRANSFER FUNCTION: Shoreline erosion due to wave impacts is routinely modeled in terms of the incoming wave energy. For wind waves, it is possible to describe impacts based on the ensemble average of many waves because the random wave characteristics are generally quasi-steady over time scales sufficient to utilize established statistical approaches. The wave packet generated by an individual vessel is much shorter in duration so that some feature of the wave envelope must be identified to form an appropriate metric to be used to represent the effects of the wave overall. The first approach is to compare the maximum force on the scarp to the maximum wave energy flux for each vessel wake packet, thus setting an upper bound on the impact force for a given vessel passage. The second approach is to compare the total energy in the wave packet to the time-integrated force, or impulse. This approach generates an estimate of the cumulative effect of all the waves in the wave train and the corresponding integrated force response for a given vessel passage.

The wave force on a vertically scarped marsh edge will be greatest when the wave breaks upon impact with the load cells. This generally occurs when water depths are between the base and midpoint of the scarp, resulting in depth-limited instabilities that cause the wave to break. For water depths below the base of the scarp such that the tidal flat is exposed, then the incoming wave

will break before impinging upon the scarp and the resulting force will be primarily due to runup. Conversely, water depths that exceed the midpoint of the scarp increase the likelihood of wave reflection and produce a surge (pulsating load) that reduces the impact force on the load cells. Thus, the same offshore wave can produce highly varied impacts depending upon the water depth, such that the relationship between force and wave energy (or energy flux) needs to account for relative water depth. This depth dependence is visible in plots of the nondimensional maximum impact force as a function of the nondimensional maximum wave energy (Figure 4a, b). The St. Augustine data in this figure are subdivided by tidal stage relative to the average height of the scarp to demonstrate that larger impact forces occur at lower relative water depths. This implies that there are more instances of wave breaking when $0.4 < h < 0.6$ m and more instances of reflection when $0.6 < h < 0.8$ m. The average force is greater when $0.4 < h < 0.6$ m, which agrees with the assumption that waves break more frequently and generate a greater impact force when the mean water depth is between the base and midpoint of the scarp. The Cocodrie results (Figure 4c) are similar to the St. Augustine results for $0.6 < h < 0.8$ (Figure 4b) in both overall range and the regression equation fitting parameters. The mean water depth at Cocodrie occurs at the mid-point of the scarp, and the tidal range is 0.1 m. Thus, all impacts occurred within +/- 0.1 m of the middle of the scarp h, so the Cocodrie data are in the reflection regime. The regression equation exponent is near 0.5 for points above the mid-point of the scarp, such that a generalized relationship indicates that, to first order, the force is proportional to the square of wave energy flux. The suggested power law relationship may provide theoretical guidance on future investigations relating the mechanics of edge erosion to wave characteristics. The non-dimensional compressive force likewise shows a general increase as a function of the non-dimensional total wave energy (Figure 4d, e, f). The St Augustine results tend to show greater spread but also greater average force when $0.4 < h < 0.6$ m.

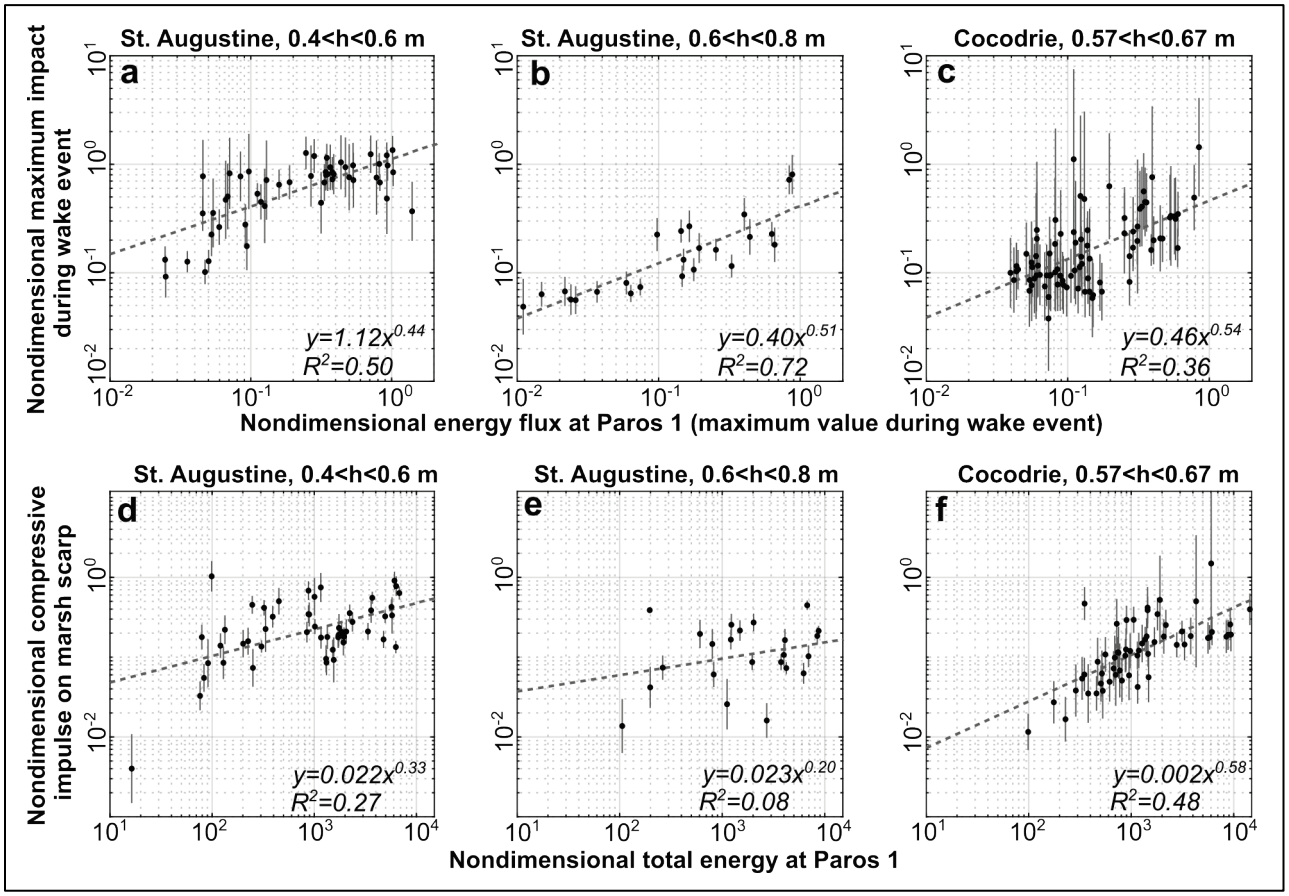

Figure 4. Relationship between nondimensional energy flux and nondimensional impact for data from (a) St. Augustine at low to mid-tide, (b) St. Augustine at mid- to high tide, and (c) Cocodrie. Relationship between nondimensional total energy and nondimensional compressive impulse for data from (d) St. Augustine at low to mid-tide, (e) St. Augustine at mid- to high tide, and (f) Cocodrie.

The transfer function based on the Cuomo et al. (2010) model shows a similar sensitivity to water surface elevation on the scarp (Figure 5), including a higher average P_{max} when $0.4 < h < 0.6$ m. When applying the model to a vertically scarped marsh edge, the Cuomo model should be adjusted to account for the change in maximum impact force due the changes in wave shoaling and breaking conditions. The dataset used to define the coefficients possesses a large degree of scatter. However, direct measurements of impact forces on scarps as a function of water surface are lacking, so the suggested parameter values represent a first order approximation and are suggested in the absence of independent data. As more data become available the parameters can be refined and modified to include a depth dependence term. The primary goal of this CHETN is to introduce the application of load cells to measuring impact forces on vertically marsh scarps and has revealed the impact force sensitivity to tidal stage.

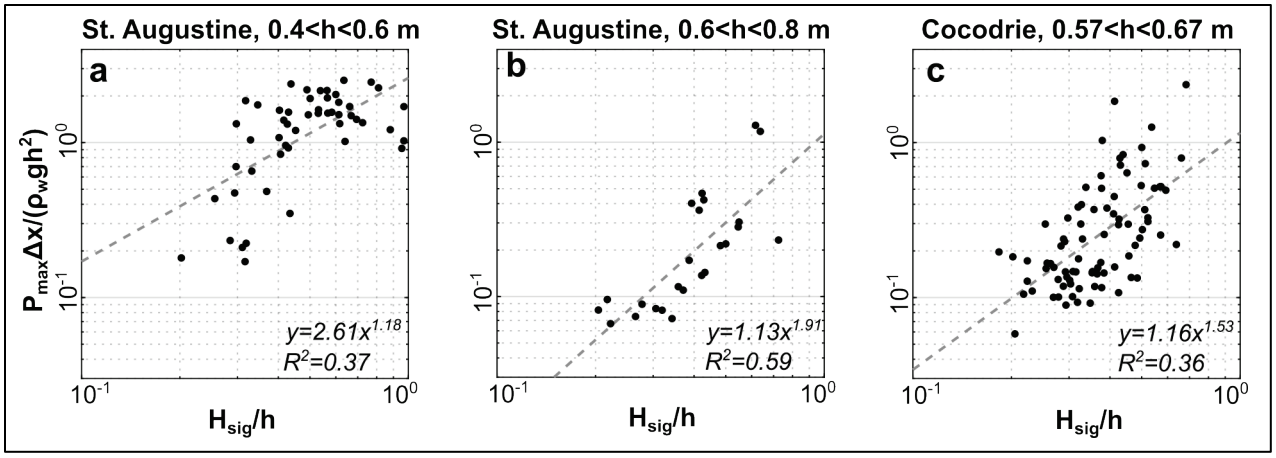

Figure 5. Relationships between wave conditions and impact forces as predicted by Cuomo et al. (2010).

ADDITIONAL INFORMATION: This CHETN was prepared as part of the US Army Corps of Engineers Navigation Systems Research Program (NavSys) by Richard Styles, US Army Engineer Research and Development Center (ERDC), Coastal and Hydraulics Laboratory (CHL), Vicksburg, MS. Questions pertaining to this CHETN may be directed to Richard Styles (*richard.styles@usace.army.mil*) or the USACE NavSys Program Manager.

This ERDC/CHL CHETN-IV-130 should be cited as follows:

> Styles R., R. L. Bain, and A. M. Priestas. 2022. *Method to Evaluate Vessel Wake Forces on Wetland Scarps.* ERDC/CHL CHETN-IV-130. Vicksburg, MS: US Army Engineer Research and Development Center. *http://dx.doi.org/10.21079/11681/45304*.

REFERENCES

Bloemendaal, Lucila, J. Houttuijn, Duncan M. FitzGerald, Zoe J. Hughes, Alyssa B. Novak, and Peter Phippen. 2021. "What Controls Marsh Edge Erosion?" *Geomorphology* 386(1): 107745.

Bridges, Todd S., et al. 2015. *Use of Natural and Nature-Based Features (NNBF) for Coastal Resilience*. ERDC SR-15-1. US Army Engineer Research and Development Center.

Burgin, Shelley, and Nigel Hardiman. 2011. "The Direct Physical, Chemical and Biotic Impacts on Australian Coastal Waters Due to Recreational Boating." *Biodiversity and Conservation* 20(4): 683–701.

Cuomo, Giovanni, William Allsop, and Shigeo Takahashi. 2010. "Scaling Wave Impact Pressures on Vertical Walls." *Coastal Engineering* 57(6): 604–609.

Gallivan, L. B., and R. A. Davis, Jr. 1981. "Sediment Transport in a Microtidal Estuary: Matanzas River, Florida." *Marine Geology* 40: 69–83.

Gedan, Keryn B., Matthew L. Kirwan, Eric Wolanski, Edward B. Barbier, and Brian R. Silliman. 2011. "The Present and Future Role of Coastal Wetland Vegetation in Protecting Shorelines: Answering Recent Challenges to the Paradigm." *Climatic Change* 106(1): 7–29.

Houser, Chris. 2010. "Relative Importance of Vessel-Generated and Wind Waves to Salt Marsh Erosion in a Restricted Fetch Environment." *Journal of Coastal Research* 26(2): 230–40.

Houser, Chris. 2011. "Sediment Resuspension by Vessel-Generated Waves along the Savannah River, Georgia." *Journal of Waterway, Port, Coastal, and Ocean Engineering* 137(5): 246–57. https://doi.org/doi:10.1061/(ASCE)WW.1943-5460.0000088.

Kumar, Pushpam. 2012. *The Economics of Ecosystems and Biodiversity: Ecological and Economic Foundations*. New York: Routledge.

Leonardi, Nicoletta, Zafer Defne, Neil K Ganju, and Sergio Fagherazzi. 2016. "Salt Marsh Erosion Rates and Boundary Features in a Shallow Bay." *Journal of Geophysical Research: Earth Surface* 121(10): 1861–75.

Marani, Marco, Andrea D'Alpaos, Stefano Lanzoni, and Marco Santalucia. 2011. "Understanding and Predicting Wave Erosion of Marsh Edges." *Geophysical Research Letters* 38(21).

Maynord, Stephen T. 2007. *Ship Forces on the Shoreline of the Savannah Harbor Project*. ERDC/CHL TR-07-7. Vicksburg, MS: US Army Engineer Research and Development Center.

Maynord, Stephen T., David S Biedenham, Craig J. Fischenich, and Jon E. Zufelt. 2008. *Boat-Wave-Induced Bank Erosion on the Kenai River, Alaska.* ERDC/CHL TR-08-05. Vicksburg, MS: US Army Engineer Research and Development Center.

McLoughlin, Sean M., Patricia L. Wiberg, Ilgar Safak, and Karen J. McGlathery. 2015. "Rates and Forcing of Marsh Edge Erosion in a Shallow Coastal Bay." *Estuaries and Coasts* 38(2): 620–38.

Oumeraci, Hocine, Andreas Kortenhaus, William Allsop, Maarten de Groot, Roger Crouch, H. Vrijling, and Hessel Voortman. 2001. *Probabilistic Design Tools for Vertical Breakwaters*. Lisse; Abingdon; Exton; Tokyo: A. A. Balkema Publishers.

Priestas, Anthony M., Giulio Mariotti, Nicoletta Leonardi, and Sergio Fagherazzi. 2015. "Coupled Wave Energy and Erosion Dynamics along a Salt Marsh Boundary, Hog Island Bay, Virginia, USA." *Journal of Marine Science and Engineering* 3(3): 1041–65.

Schwimmer, Reed A. 2001. "Rates and Processes of Marsh Shoreline Erosion in Rehoboth Bay, Delaware, USA." *Journal of Coastal Research* 17(3) Summer 2001: 672–683.

Sorensen, Robert M. 1997. *Prediction of Vessel-Generated Waves with Reference to Vessels Common to the Upper Mississippi River System*. ENV Report 4. Rock Island: US Army Corps of Engineers.

Styles, Richard, and Michael A. Hartman. 2018. *Wave Characteristics and Sediment Resuspension by Recreational Vessels in Coastal Plain Saltmarshes*. ERDC/CHL TR-18-5. Vicksburg, MS: US Army Engineer Research and Development Center.

Tonelli, Mara, Sergio Fagherazzi, and Marco Petti. 2010. "Modeling Wave Impact on Salt Marsh Boundaries." *Journal of Geophysical Research: Oceans* 115(C9): 1–17.

Wamsley, Ty V., Mary A. Cialone, Jane M. Smith, John H. Atkinson, and Julie D. Rosati. 2010. "The Potential of Wetlands in Reducing Storm Surge." *Ocean Engineering* 37(1): 59–68.